American Mineralogist, Volume 73, pages 1325–1334, 1988

Mechanism of illite formation during smectite-to-illite conversion in a hydrothermal system

ATSUYUKI INOUE*
Laboratoire de Pétrologie des Altérations Hydrothermales, Université de Poitiers, UA721 CNRS, 40, Avenue du Recteur Pineau, 86022 Poitiers Cedex, France

BRUCE VELDE
Laboratoire de Géologie, Ecole Normale Supérieure, ER224 CNRS, 46, Rue d'Ulm, 752230 Paris Cedex 05, France

ALAIN MEUNIER
Laboratoire de Pétrologie des Altérations Hydrothermales, Université de Poitiers, UA721 CNRS, 40, Avenue du Recteur Pineau, 86022 Poitiers Cedex, France

GERARD TOUCHARD
Laboratoire de Physiques et Mecanique Fluids, Université de Poitiers, UA191 CNRS, 40, Avenue du Recteur Pineau, 86022 Poitiers Cedex, France

ABSTRACT

Grain size was measured on interstratified illite/smectite (I/S) with 55–0% expandable layers and of hydrothermal origin. The grain-length and grain-width histograms vary systematically as functions of percent expandable layers, and the length and width distributions normalized to the modes give steady-state profiles. These observations convincingly prove that coarsening in the lateral faces of I/S particles in the hydrothermal setting examined is controlled by an Ostwald ripening process. The shape of steady-state profiles also shows that a spiral-growth mechanism dominates the growth of the I/S minerals.

The growth of the I/S minerals occurs in two stages. One is the growth of lath-shaped particles present in I/S with 55–20% expandable layers. This stage can continue metastably up to 0% expandable layers. The second stage is the growth of hexagonal particles in I/S with 20–0% expandable layers. The first stage corresponds to the evolution from $1M_d$ to $1M$ illite and the second to the evolution of $2M_1$ illite. The growth of both particle types can be described by the same Ostwald ripening mechanism. The polytypic transformation from $1M$ to $2M_1$ that occurs between 20% and 12% expandable layers probably requires dissolution of lath particles having a $1M$ polytype.

INTRODUCTION

Smectite-to-illite conversion is an important mineralogical reaction that occurs during the diagenesis of argillaceous sediments (Burst, 1959; Perry and Hower, 1970; Dunoyer de Segonzac, 1970; Weaver and Beck, 1971; Foscolos and Kodama, 1974; Hower et al., 1976; Boles and Franks, 1979; Hoffman and Hower, 1979; Hower, 1981). This conversion is also important to an understanding of hydrothermal alteration, especially the thermal history of rocks in active and fossil geothermal fields (Steiner, 1968; Muffler and White, 1969; Browne and Ellis, 1970; Eslinger and Savin, 1973; Inoue et al., 1978; McDowell and Elders, 1980; Inoue and Utada, 1983; Horton, 1985; Jennings and Thompson, 1986). Although the conversion of smectite to illite has been well documented, the mechanism of the conversion is still controversial. Hower et al. (1976) proposed a continuous transformation of smectite to illite by means of cation substitution in precursor smectite layers; this process has been called a solid-state transformation mechanism. In contrast, Nadeau et al. (1985) advocated a mechanism of stepwise dissolution and recrystallization. Inoue (1986) and Inoue et al. (1987) used scanning and transmission electron microscopic data for a series of I/S minerals of hydrothermal origin to support the dissolution and recrystallization mechanism. According to Inoue et al. (1987), randomly interstratified I/S grains with 100–50% expandable layers are smectites that are undergoing K fixation and grain dissolution, and short- and long-range–ordered I/S grains with 50–0% expandable layers are immature illites that are still growing. An understanding of the smectite-to-illite conversion requires an understanding of the mechanisms and kinetics of smectite dissolution and illite growth in a given natural environment. The purpose of the present paper is to describe the mechanism of illite growth during the smectite-to-illite conversion for I/S with 50–0% expandable layers.

* Present address: Geological Institute, College of Arts and Sciences, Chiba University, Chiba 260, Japan.

0003–004X/88/1112–1325$02.00

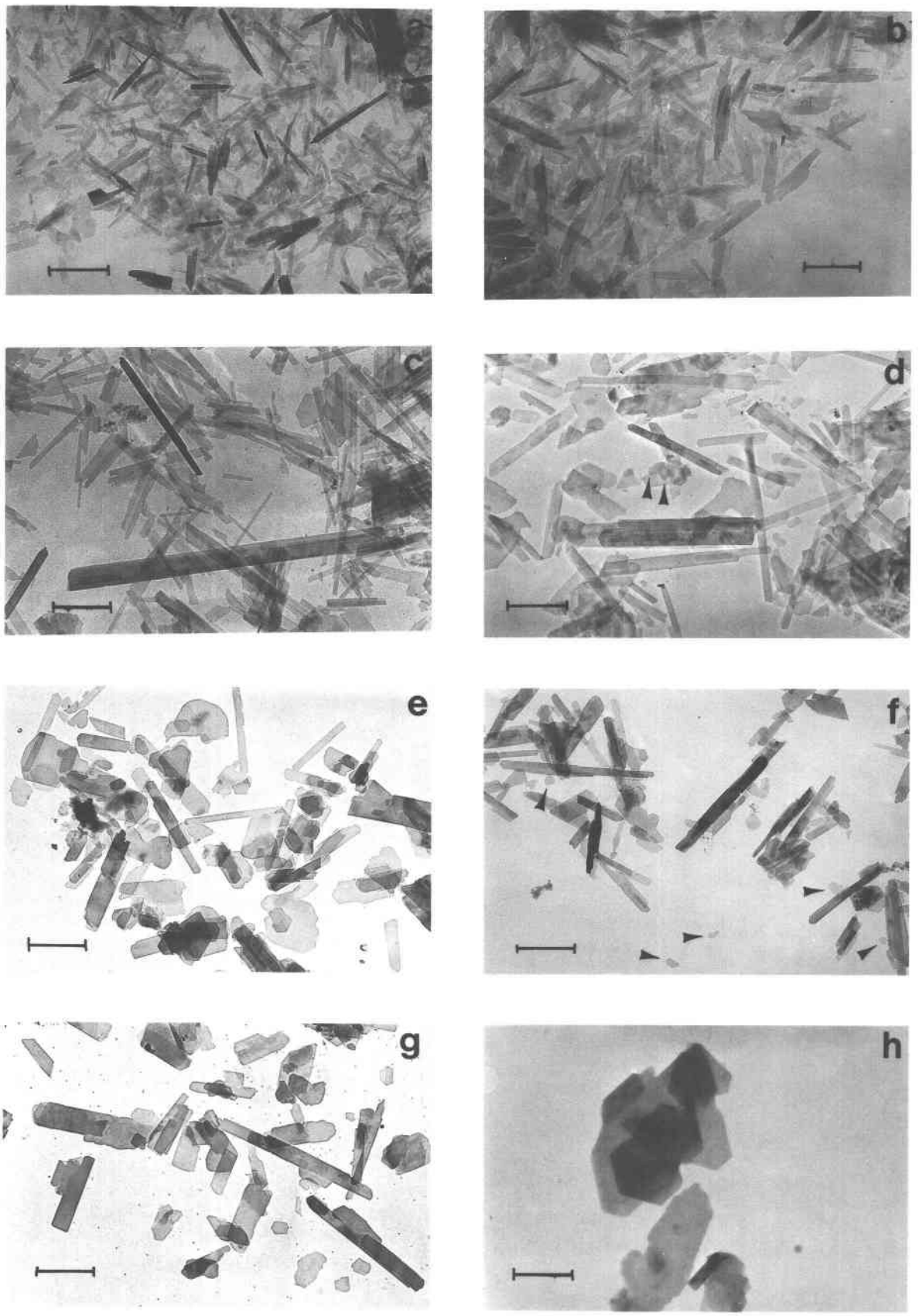
a
b
c
d
e
f
g
h

Baronnet (1974, 1982, 1984) showed that micas in high-temperature and high-pressure autoclave experiments (600 °C, 1 kbar) grow by both ripening and coalescence and that the growth can be described by Ostwald ripening. According to Baronnet (1982), Ostwald ripening is characterized by the simultaneous growth and dissolution of grains in a closed system. After nucleation, a system may contain a large number of crystallites with different sizes. The tendency then is to minimize surface free energy by dissolving small particles and growing large particles via material transfer from the former to the latter, based upon the well-known Gibbs-Thomson relation. The coalescence phenomenon involves a discontinuous increase of size of individual crystals accompanied by a decrease of their total number. In systems in which growth is controlled by Ostwald ripening, grain-size histograms broaden, flatten, and shift toward greater size with time (Nielsen, 1964). Grain-size distributions normalized to the modes in the histograms typically have a steady-state shape (Lifshitz and Slyozov, 1961; Wagner, 1961; Exner and Lukas, 1971; Chai, 1973). Baronnet (1982) pointed out that natural clays could grow by the Ostwald ripening mechanism, but little work has been done to investigate this possibility. To examine whether Ostwald ripening describes I/S reactions, we have carried out grain-size analysis for a series of I/S minerals from the Shinzan, Japan, hydrothermal area previously studied by Inoue (1986) and Inoue et al. (1987).

Samples and experimental methods

Samples

In the present study, nine samples of I/S from the Shinzan alteration area (Akita Prefecture, Japan) were used (Table 1). These samples have previously been described by Inoue et al. (1978), Inoue and Utada (1983), Inoue (1986), and Inoue et al. (1987). The percent expandable layers in these samples are between 55% and 0%, and the ordering type (Reichweite: g) ranges from random interstratification ($g = 0$) to pure illite through short- and long-range–ordered interstratifications ($g = 1$, 2, and ≥ 3). The definition of Reichweite follows that of Jagodzinski (1949). Transmission-electron micrographs of these samples are shown in Figure 1. The randomly interstratified samples contain clay particles with a thin lathlike habit coexisting with more abundant flakes. The flaky and lathlike particles correspond to randomly interstratified I/S and short-range–ordered clays, respectively (Inoue et al., 1987). In samples with 40–20% expandable layers, the particles are chiefly thin laths. In samples with 15–12% expandable layers, there are tiny hexagonal or lozenge-shaped particles (<0.2 μm in length), together with lath-shaped ones (Fig. 1). The pure illite contains plates with hexagonal habits together with laths wider than 0.1 μm. The K contents of the lath- and hexagonal-shaped samples range from 0.29 to 0.80 ions per half formula unit.

Table 1. Percent expandable layers, ordering type, and K content in interstratified I/S

Sample	Expandable layers (%)	Ordering (Reichweite)	$K/O_{10}(OH)_2$
WS-2-383	55 ± 5	0	0.29 ± 0.07
WS-4-392	50 ± 10	0	0.31 ± 0.09
WS-2-423	40 ± 5	1	0.34 ± 0.07
WS-4-440	30 ± 5	1	0.43 ± 0.10
WS-5-240	20 ± 5	2	0.71 ± 0.02
WS-7-115	15 ± 5	≥3	
WS-5-185	12 ± 3	≥3	0.73 ± 0.06
WS-7-197	5 ± 5	≥3	0.76 ± 0.06
WS-8-452	0		0.80 ± 0.01

Methods

Transmission electron microscopic (TEM) examination was made with a JEOL 100SX transmission electron microscope on clay fractions (<1 μm) of each sample, which were newly isolated from the rock materials by centrifugation and dispersal in deionized water by means of ultrasonic vibration. This preparation was deposited on C-coated Cu grids. The proper concentration of clay suspension to obtain good dispersion on a grid was determined by trial and error.

For samples with 55–50% expandable layers, only lath-shaped particles were measured for grain size. The flakes were neglected, because only the laths correspond to illitic mineral, as mentioned above. In the other samples, all the particle types were measured. The particle sizes and shapes were measured using a digitizing table. The corners of a polygonal particle were marked with the stylus. The length (L), width (W), and aspect ratio (R) were then calculated. The particle length is defined as the longest distance parallel to the longest edge of a particle. The width is defined as the longest distance perpendicular to the direction of the length. The aspect ratio, R, is defined as the value of L/W.

The percent expandable layers of each sample was determined by applying the $\Delta 2\theta_1 - \Delta 2\theta_2$ diagram of Watanabe (1981) to X-ray powder diffraction (XRD) patterns of glycolated samples (see Inoue and Utada, 1983; Inoue et al., 1987). The accuracy of the determination of percent expandable layers is ±5% for most I/S samples.

Chemical analysis of I/S particles was made with a Hitachi H-500 transmission electron microscope equipped with a Kevex 5000 solid-state detector for energy-dispersive X-ray analysis and a microcomputer for quantitative data processing (Inoue et al., 1987). The accelerating voltage and beam current were 100 kV and about 240 pA, respectively. The measured X-ray intensity of each element was corrected by using the methods of Cliff and Lorimer (1975) and using k values obtained from standard clay specimens (kaolinite, muscovite, celadonite, and chlorite). For a quantitative analysis, particles with a thickness of at least a few hundred angstrom units were used to obtain useful X-ray signal/noise ratios.

←

Fig. 1. Transmission-electron micrographs of illite/smectite with (**a**) 50% expandable layers, (**b**) 40% expandable layers, (**c**) 30% expandable layers, (**d**) 20% expandable layers, (**e**) 15% expandable layers, (**f**) 12% expandable layers, (**g**) 5% expandable layers, and (**h**) 0% expandable layers. The scale bars are 0.5 μm. Tiny hexagonal and lozenge-shaped particles are indicated by arrows.

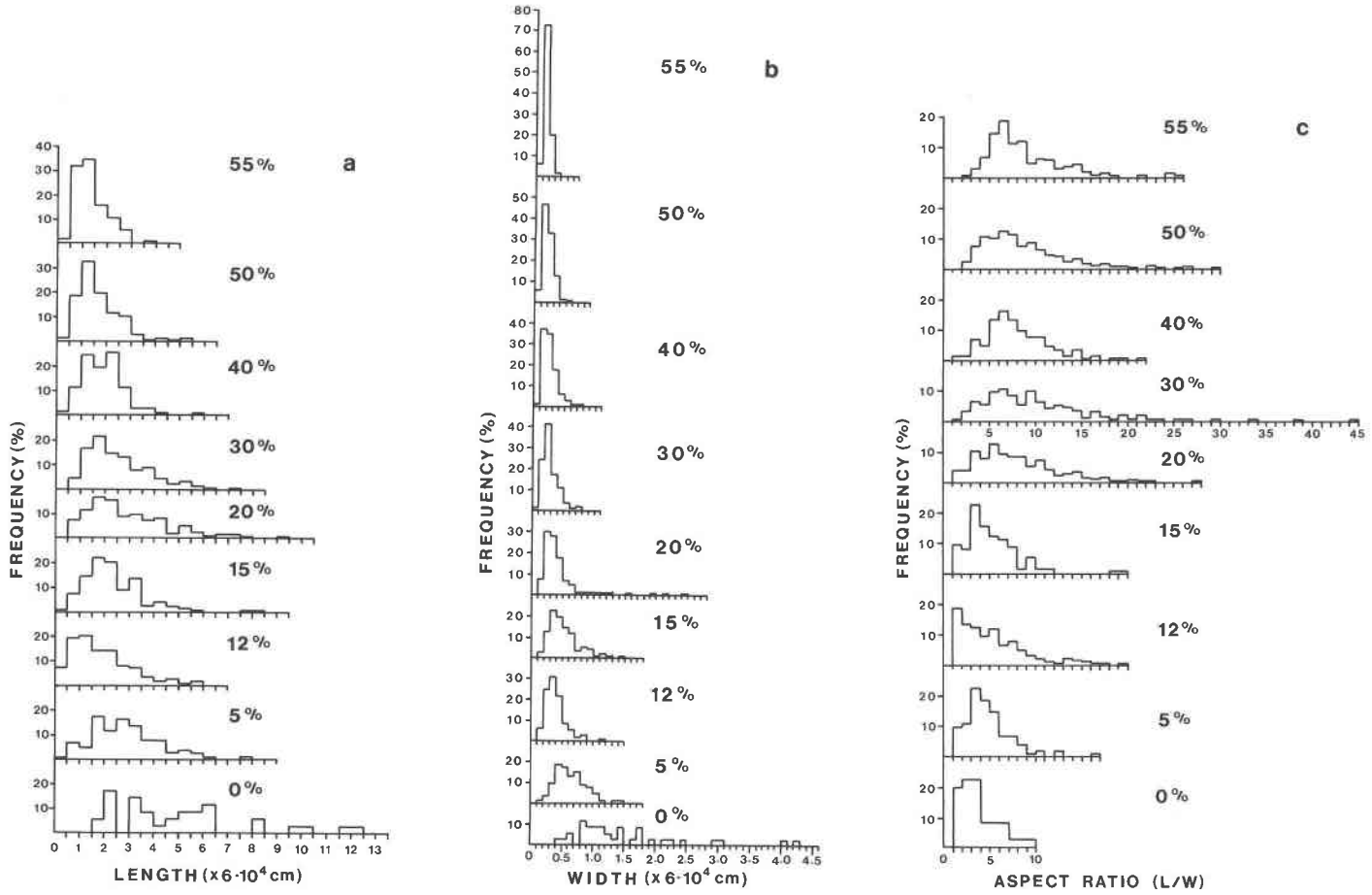

Fig. 2. **(a)** Length histograms for illite/smectite as functions of percent expandable layers. **(b)** Width histograms for illite/smectite as functions of percent expandable layers. **(c)** Aspect-ratio histograms for illite/smectite as functions of percent expandable layers.

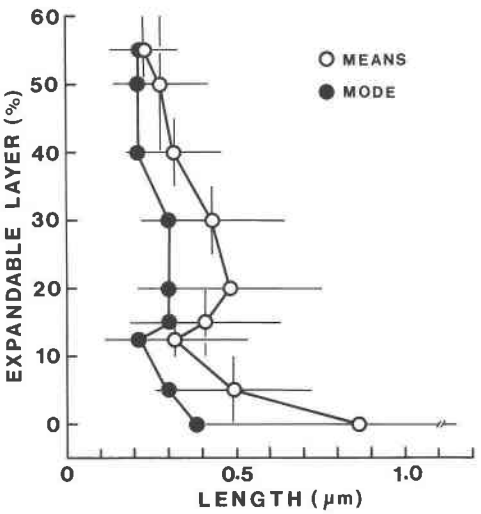

Fig. 3. Length as a function of percent expandable layers.

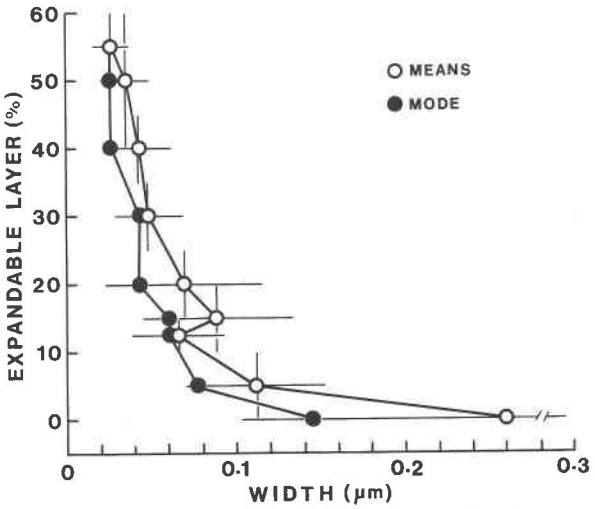

Fig. 4. Width as a function of percent expandable layers.

Results

Histograms of length, width, and aspect ratio for samples with different percent expandable layers are shown in Figures 2a, 2b, and 2c, respectively. The means, modes, and observed maximum values of the length, width, and aspect ratio are summarized in Table 2.

Grain-length distribution

As shown in Figure 2a, the grain-length histograms for I/S with 55–50% expandable layers have an asymmetrical distribution and become more symmetrical with decreasing percent expandable layers. In addition, these histograms broaden and flatten with decreasing percent expandable layers. The mean length and the mode increase with decreasing percent expandable layers in the range of 55–30%, then decrease in the range of 20–12% expandable layers, and increase again in the range of 12–0% (Fig. 3).

Grain-width distribution

The grain-width distributions of the samples with more expandable layers are narrow, but become broader with decreasing percent expandable layers (Fig. 2b). The mean value increases with decreasing percent expandable layers in the range of 55–15%, slightly decreases at 12%, and then significantly increases in the range of 12–0% (Fig. 4). These features are similar to those of the grain-length distribution.

Aspect-ratio distribution

The aspect-ratio distributions broaden and flatten with decreasing percent expandable layers in the range of 55–30%, but become asymmetrical, sharpen, and shift toward smaller values with decreasing percent expandable layers (Figs. 2c and 5). The aspect-ratio mode is approximately constant at 6.5 in the range of 55–30% expandable layers and decreases with decreasing percent expandable layers (Fig. 5). The increase in length and width values in the range of 55–30% (Figs. 3 and 4) means that morphologically anisotropic lath particles were growing in this range such that they keep a constant aspect ratio. The decrease in aspect-ratio value in the range of 20–12% expandable layers may be due to two factors: growth of lath-shaped particles toward a more equant form or the nucleation and growth of new, more equant particles. In

Table 2. Length, width, and aspect ratio obtained from grain-size analysis of interstratified illite/smectite

Sample	Measured particle	Length (μm)			Width (μm)			Aspect ratio		
		Mean (STD)	Mode	Max	Mean (STD)	Mode	Max	Mean (STD)	Mode	Max
WS-2-383	168	0.23 (0.10)	0.21	0.61	0.027 (0.010)	0.026	0.053	8.73 (4.02)	6.5	25.9
WS-4-392	279	0.28 (0.14)	0.21	0.99	0.035 (0.014)	0.026	0.098	8.77 (4.65)	6.5	29.0
WS-2-423	143	0.32 (0.14)	0.21	0.96	0.043 (0.019)	0.026	0.121	8.13 (3.56)	6.5	21.9
WS-4-440	191	0.43 (0.21)	0.30	1.20	0.048 (0.020)	0.043	0.127	10.15 (6.34)	6.5	44.1
WS-5-240	267	0.48 (0.27)	0.30	1.54	0.069 (0.046)	0.043	0.416	8.02 (4.45)	5.5	27.1
WS-7-115	124	0.41 (0.22)	0.30	1.37	0.088 (0.043)	0.060	0.253	5.26 (2.98)	3.5	19.5
WS-5-185	239	0.32 (0.21)	0.21	0.98	0.066 (0.027)	0.060	0.186	5.36 (3.65)	1.5	19.5
WS-7-197	102	0.49 (0.23)	0.30	1.30	0.111 (0.041)	0.077	0.222	4.81 (2.54)	3.5	16.6
WS-8-452	35	0.86 (0.47)	0.38	2.12	0.260 (0.156)	0.145	0.732	3.81 (2.10)	3	9.8

Note: STD means the standard deviation.

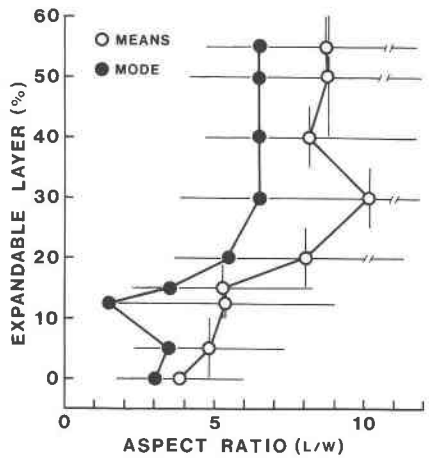

Fig. 5. Aspect ratio as a function of percent expandable layers.

fact, many tiny hexagonal or lozenge-shaped particles coexist with lath-shaped particles in the samples having less than 15% expandable layers (Fig. 1). The theoretical R value of an ideal hexagon is 1.15. Therefore, the decrease in R value at about 12% expandable layers is due to the appearance of tiny hexagonal or lozenge-shaped particles. This observation is consistent with the decrease in L and W values at about 12% expandable layers, as mentioned previously.

Discussion

Growth mechanism of illite

As discussed above, Ostwald ripening predicts that grain-size histograms broaden, flatten, and shift toward greater size with time. In the present study, the length and width histograms change as a function of percent expandable layers instead of time. This observation supports but does not prove a ripening mechanism for the growth of the illitic minerals examined here.

Ostwald ripening theory predicts that when a grain-size histogram is plotted in reduced coordinates, such as $f(r)/f(r)_{max}$ and $r/\bar{r}$, in which the grain-size distribution is normalized to the mode, the distribution forms a steady-state profile (Lifshitz and Slyozov, 1961; Wagner, 1961; Exner and Lukas, 1971; Chai, 1973; Baronnet, 1982, 1984). Here $f(r)$ and $f(r)_{max}$ are the frequency of a given grain size and the maximum frequency encountered, and r and $\bar{r}$ are the grain size and the mean grain size, respectively. Such steady-state profiles are independent of ripening time and initial grain-size distribution. The shape of a steady-state profile is indicative of the type of the growth-controlling mechanism (Baronnet, 1982, 1984). Grain-size distributions normalized to the modes of the lengths and widths of our I/S samples as functions of percent expandable layers have steady-state profiles (Figs. 6 and 7). In these diagrams, the data for the 0% expandable layers sample were omitted, because the number of particles measured is too small (35 grains) compared to the others (>100 grains), and therefore the definition of the grain-size distribution is statistically poor (Fig. 2). Both steady-state profiles are characterized by a maximum value of about 0.8 with respect to $L/\bar{L}$ and $W/\bar{W}$ and by the tailing of profile toward greater $L/\bar{L}$ and $W/\bar{W}$ values.

According to Baronnet (1982), the ripening process involves three kinetic steps, i.e., dissolution, solute transfer, and growth. The growth step is generally rate limiting in Ostwald ripening kinetics. The growth rate of crystal particles at a constant temperature can be expressed by

$$dr/dt = K\sigma_r^n,$$

where K = growth-rate constant, σ_r = relative supersaturation of the bulk solution with respect to a particle size r, and $1 \leq n \leq 2$, where n = the order of the kinetics.

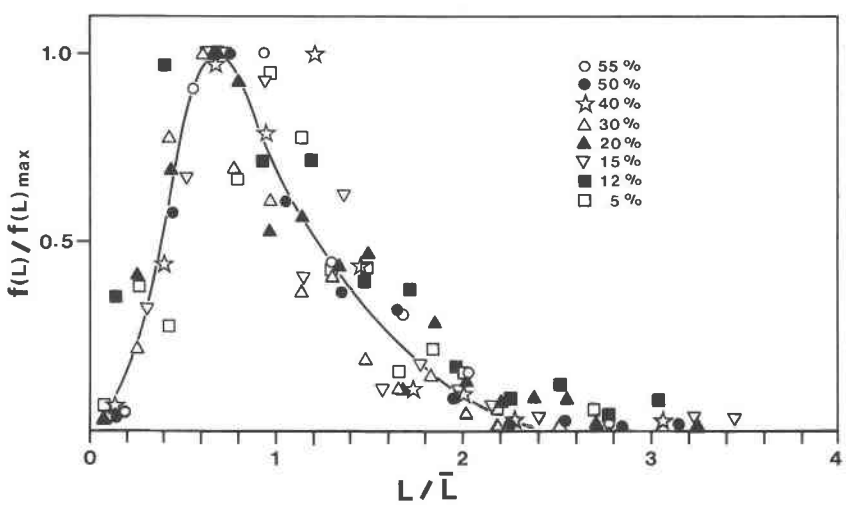

Fig. 6. Length of illite/smectite grains normalized to the mode as a function of percent expandable layers. The curve has been smoothed.

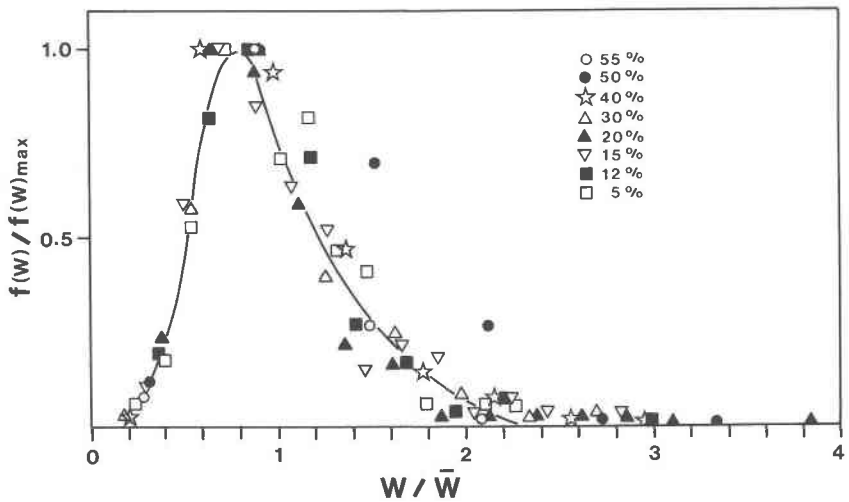

Fig. 7. Width of illite/smectite grains normalized to the mode as a function of percent expandable layers. The curve has been smoothed.

Boundary cases $n = 1$ and 2 are accounted for by the BCF theory of spiral growth (Burton et al., 1951) of crystal faces controlled by a screw-dislocation mechanism. The first- and second-order kinetics operate under high- and low-supersaturation conditions, respectively. Volume diffusion-controlled ripening predicts the second-order kinetics as well (Greenwood, 1956). The present steady-state profiles for length and width fit exceedingly well the theoretical profile for a spiral-growth mechanism under low-supersaturation conditions (second-order kinetics; Fig. 8). No spiral patterns have yet been observed on the lateral faces of micas (Baronnet, 1984). However, Sun and Baronnet (pers. comm.) recently demonstrated from measurements of growth rates of synthetic mica single crystals that the lateral faces grow according to the same spiral-growth mechanism as that on the basal faces.

Inoue et al. (1987) measured the thickness distribution of some of the present specimens by a Pt-Pd shadowing method. These thickness data do not give a steady-state profile because of the small number of data. No spiral growth patterns were observed on the basal faces of these samples. Nevertheless, it is reasonable to assume that the growth on the basal faces followed the same Ostwald ripening process as the other directions, probably controlled by a spiral-growth mechanism. K-Ar dating of the samples (our unpub. data) shows that the ripening occurred about 1 Ma in the present hydrothermal setting.

Crystallization generally involves both nucleation and crystal-growth processes. All the I/S samples studied here, except the 0% expandable layer sample, have attained a steady state in their growth. TEM observations show that in the studied I/S samples, nucleation of lath-shaped par-

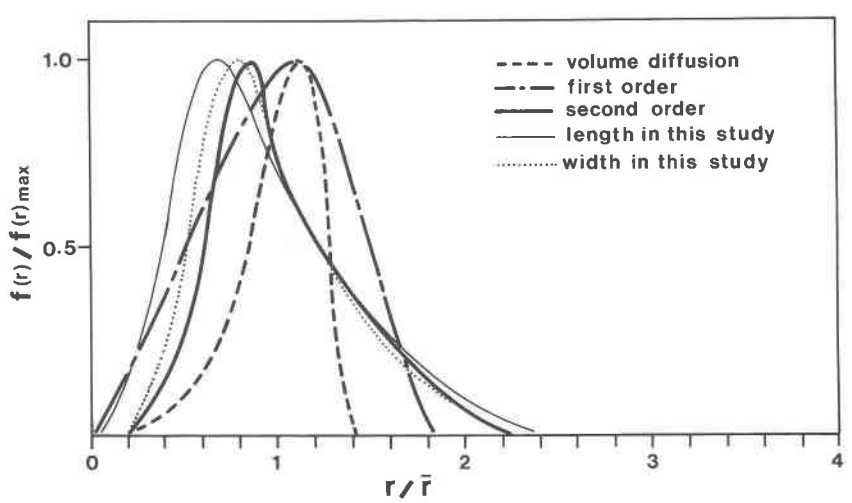

Fig. 8. Comparison of the experimental curves (Figs. 6 and 7) with theoretical steady-state profiles calculated for various growth-controlling mechanisms (see text).

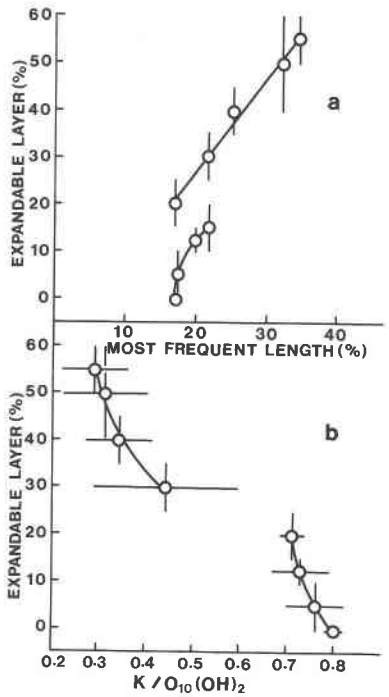

Fig. 9. (a) Relationship between the percent expandable layers and the percent of all grains with the most frequent length (mode) in illite/smectite. (b) Relationship between the percent expandable layers and the K content per half formula unit in illite/smectite.

ticles began at the stage when the I/S contained more than 55% expandable layers (Inoue et al., 1987). Nucleation of the hexagonal particles apparently started at about 20% expandable layers, because many tiny hexagonal particles occur in samples with 15–12% expandable layers.

1M-to-$2M_1$ illite polytypic transformation

The growth of illitic minerals during smectite-to-illite conversion in this hydrothermal setting consists of two distinct growth sequences (Fig. 9). One corresponds to growth of laths between 55% and 20% expandable layers, and the other to that of the hexagonal-shaped crystals between 20% and 0% expandable layers. Previous XRD and TEM examinations indicate that the lath-shaped illite has $1M_d$ or *1M* symmetry and the hexagonal illite has $2M_1$ symmetry (Inoue et al., 1987). Therefore, the size discontinuity in the growth evolution of illite particles is related to the *1M*-to-$2M_1$ polytypic transformation.

Several hypotheses have been proposed for the mechanism of the *1M*-to-$2M_1$ polytypic transformation in muscovite, e.g., lattice reconstruction in the solid state (Hunziker et al., 1986) and dissolution-recrystallization (Baronnet, 1980; Mukhamet-Galeyer et al., 1985). Baronnet (1980) assumed the *1M*-to-$2M_1$ transformation in high-temperature and high-pressure hydrothermal experiments to take place by a ripening process at a constant temperature as follows: During an initial nucleation stage, a large number of $1M_d$ mica particles form; the grain-size distribution is characterized by a very dispersed aspect-ratio distribution. When the bulk supersaturation in the solution decreases, the particles smaller than the critical size dissolve to form *1M* overgrowths on the larger $1M_d$ particles. With further decrease in supersaturation, the dissolving, smaller *1M* particles feed $2M_1$ overgrowths on the larger *1M* particles. According to this hypothesis, the transformation cannot go fully to completion, because the cores of the continually growing crystals record and retain all the successive growth forms from the nucleation stage. In other words, we can observe the three types of mica modification ($1M_d$, *1M*, and $2M_1$) in one large, thick crystal. The variations in the length and width of the natural I/S minerals of the present study (Figs. 3 and 4), which presumably occurred under nonisothermal conditions, however, suggest that dissolution of large laths and the formation of the small hexagons occur during the *1M*-to-$2M_1$ transformation. Such dissolution-recrystallization during the *1M*-to-$2M_1$ polytypic transformation has been emphasized by Mukhamet-Galeyer et al. (1985) on the basis of TEM observations of the morphology of synthetic muscovite.

The present *1M*-to-$2M_1$ polytypic transformation process at the Shinzan area may be summarized as follows. The initially nucleated laths with the $1M_d$ or *1M* polytype grew dominantly in two dimensions, keeping a nearly constant aspect ratio in the range between 55% and 20% expandable layers. Laths larger than the critical size for the actual fluid supersaturation continued to grow metastably up to the 0% expandable layer stage, although the aspect ratio may have decreased slightly. The $2M_1$ hexagonal crystals began to form at about 20% expandable layers, with dissolution of laths occurring at between 20% and 12% expandable layers. Growth of hexagonal crystals tended to a more equant shape, increasing the aspect ratio and thickness slightly.

Figure 9b shows that a large change in the K content of the samples correlates with the change from the *1M* to $2M_1$ polytype at about 20% expandable layers. Thus, the two polytypes have different chemical compositions, in addition to different morphologies and growth dynamics, especially in their early crystallization stages. The K content of the laths gradually increases with growth, whereas the K content of the hexagons is more nearly constant at 0.7–0.8 ions per half formula unit. The overall transformation observed in the present study is $1M_d \rightarrow 1M \rightarrow 2M_1$, consistent with the previous observations made on synthetic experiments of muscovite (Yoder and Eugster, 1955; Smith and Yoder, 1956; Velde, 1965).

Summary and conclusions

Grain-size analysis of interstratified I/S confirms the following conclusions regarding the mechanism of illite formation during smectite-to-illite conversion in hydrothermal systems.

1. The coarsening of illitic minerals in the lateral faces and possibly basal faces follows an Ostwald ripening pro-

cess in which the growth rate is probably controlled by a spiral-growth mechanism. The present data indicate that I/S minerals with less than 55% expandable layers have attained to a steady state in their growth. The nucleation of particles having a lath-shaped habit begins rather early in the smectite-to-illite conversion, possibly at 80–70% expandable layers.

2. The growth of illitic minerals during the smectite-to-illite conversion from 55% to 0% expandable layers consists of two processes: growth of lath-shaped particles having $1M_d$ or $1M$ symmetry and the nucleation and growth of hexagonal-shaped particles having $2M_1$ symmetry. The growth of $1M$ crystals takes place in the range of 55–20% and continues metastably up to 0% expandable layers, whereas $2M_1$ crystals begin to form at about 20% expandable layers. The development of $2M_1$ illite probably occurs simultaneously with dissolution of $1M$ laths between 20% and 12% expandable layers. The coarsening of both crystal populations is controlled by Ostwald ripening. These two polytypes have different interlayer K contents in addition to different morphology, especially in their early crystallization stages.

Acknowledgments

We greatly thank A. Baronnet, Université de Aix-Marseille III, and D. Beaufort, Université de Poitiers, for their valuable suggestions in the process of completing this study and critical reading of the manuscript.

References cited

Baronnet, A. (1974) Étude en microscopie électronique des premiers stades de croissance d'un mica synthétique, la phlogopite hydroxylée. Phénomènes de coalescence et de murissement dans le systeme fermé conservatif: K_2O–$6MgO$–Al_2O_3–$6SiO_2$–excès H_2O. High Temperature and High Pressure, 6, 675–685.

——— (1980) Polytypism in micas: A survey with emphasis on the crystal growth aspect. In E. Kaldis, Ed., Current topics in material science, vol. 5, p. 447–548. North Holland, Amsterdam.

——— (1982) Ostwald ripening in solution. The case of calcite and mica. Estudios Geologicos, 38, 185–198.

——— (1984) Growth kinetics of the silicates. A review of basic concepts. Fortschritte der Mineralogie, 62, 187–232.

Boles, J.R., and Franks. S.G. (1979) Clay diagenesis in Wilcox sandstones of southwest Texas: Implications of smectite diagenesis on sandstone cementation. Journal of Sedimentary Petrology, 49, 55–70.

Browne, P.R.L., and Ellis, A.J. (1970) The Ohaki-Broadlands hydrothermal area, New Zealand: Mineralogy and related geochemistry. American Journal of Science, 269, 97–131.

Burst, J.F., Jr. (1959) Post-diagenetic clay mineral environmental relationships in the Gulf Coast Eocene. Clays and Clay Minerals, 6, 327–341.

Burton, W.K., Cabrera, N., and Frank, F.C. (1951) The growth of crystals and the equilibrium structure of their faces. Philosophical Transactions of the Royal Society, 243, 299–358.

Chai, B.H.T. (1973) Mass transfer of calcite during hydrothermal recrystallization. In A.W. Hofmann, B.J. Giletti, H.S. Yoder, Jr., and R.A. Yund, Eds., Geochemical transport and kinetics. Carnegie Institution of Washington Publication 634, 205–218.

Cliff, G., and Lorimer, G.W. (1975) The quantitative analysis of thin specimens. Journal of Microscopy, 103, 203–207.

Dunoyer de Segonzac, G. (1970) The transformation of clay minerals during diagenesis and low-grade metamorphism: A review. Sedimentology, 15, 281–346.

Eslinger, E.V., and Savin, S.M. (1973) Mineralogy and oxygen isotope geochemistry of the hydrothermally altered rocks of the Ohaki-Broadlands, New Zealand, geothermal area. American Journal of Science, 273, 240–267.

Exner, H.E., and Lukas, H.L. (1971) The experimental verification of the stationary Wagner-Lifshitz distribution of coarse particles. Metallography, 4, 325–338.

Foscolos, A.F., and Kodama, H. (1974) Diagenesis of clay minerals from lower Cretaceous shales of northeastern British Columbia. Clays and Clay Minerals, 22, 319–336.

Greenwood, G.W. (1956) The growth of dispersed precipitates in solutions. Acta Metallurgica, 4, 243–248.

Hoffman, J., and Hower, J. (1979) Clay mineral assemblages as low grade metamorphic geothermometers: Application to the thrust-faulted Disturbed belt of Montana, U.S.A. Society of Economic Geology, Paleontology, and Mineralogy Special Publication 26, 55–79.

Horton, D.G. (1985) Mixed-layer illite/smectite as a paleotemperature indicator in the Amethyst vein system, Creede district, Colorado, USA. Contributions to Mineralogy and Petrology, 91, 171–179.

Hower, J. (1981) Shale diagenesis. Mineralogical Association of Canada, Short Course Handbook 7, 60–80.

Hower, J., Eslinger, E., Hower, M., and Perry, E. (1976) The mechanism of burial diagenetic reactions in argillaceous sediments: 1. Mineralogical and chemical evidence. Geological Society of America Bulletin, 87, 725–737.

Hunziker, J.C., Frey, M., Clauer, N., Dallmeyer, R.D., Friedrichsen, H., Flehmig, W., Hochstrasser, K., Roggwiler, P., and Schwander, H. (1986) The evolution of illite to muscovite: Mineralogical and isotopic data from the Glarus Alps, Switzerland. Contributions to Mineralogy and Petrology, 92, 157–180.

Inoue, A. (1986) Morphological change in a continuous smectite-to-illite conversion series by scanning and transmission electron microscopies. Journal of College of Arts and Sciences, Chiba University, B-19, 23–33.

Inoue, A., and Utada, M. (1983) Further investigations of a conversion series of dioctahedral mica/smectites in the Shinzan hydrothermal alteration area, northeast Japan. Clays and Clay Minerals, 31, 401–412.

Inoue, A., Minato, H., and Utada, M. (1978) Mineralogical properties and occurrence of illite/montmorillonite mixed layer minerals formed from Miocene volcanic glass in Waga-Omono district. Clay Science, 5, 123–136.

Inoue, A., Kohyama, N., Kitagawa, R., and Watanabe, T. (1987) Chemical and morphological evidence for the conversion of smectite to illite. Clays and Clay Minerals, 35, 111–120.

Jagodzinski, H. (1949) Eindimensinale Fehlordnung in Kristallen und ihr Einfluss auf die Röntgeninterferenzed. I. Berechnung des Fehlordnungsgrades aus der Röntgenintensitaten. Acta Crystallographica, 2, 201–207.

Jennings, S., and Thompson, G.R. (1986) Diagenesis in Plio-Pleistocene sediments in the Colorado River delta, southern California. Journal of Sedimentary Petrology, 56, 89–98.

Lifshitz, I.M., and Slyozov, V.V. (1961) The kinetics of precipitation from supersaturated solid solutions. Journal of Physics and Chemistry of Solids, 19, 35–50.

McDowell, D.S., and Elders, W.A. (1980) Authigenic layer silicate minerals in borehole Elmore 1, Salton Sea geothermal fields, California, U.S.A. Contributions to Mineralogy and Petrology, 74, 293–310.

Muffler, L.J.P., and White, D.E. (1969) Active metamorphism of upper Cenozoic sediments in the Salton Sea geothermal fields and the Salton trough, southeastern California. Geological Society of America Bulletin, 80, 157–182.

Mukhamet-Galeyer, A.P., Pokrovskiy, V.A., Zotov, A.V., Ivanov, I.P., and Samotoin, N.D. (1985) Kinetics and mechanism of hydrothermal crystallization of $2M_1$ muscovite: An experimental study. International Geology Review, 27, 1357–1364.

Nadeau, P.H., Wilson, M.J., McHardy, W.J., and Tait, J.W. (1985) The conversion of smectite to illite during diagenesis: Evidence from some illitic clays from bentonites and sandstones. Mineralogical Magazine, 49, 393–400.

Nielsen, A.E. (1964) Kinetics of precipitation, p. 108–119. Pergamon Press, New York.

Perry, E., and Hower, J. (1970) Burial diagenesis in Gulf Coast pelitic sediments. Clays and Clay Minerals, 18, 165–177.

Smith, J.V., and Yoder, H.S., Jr. (1956) Experimental and theoretical studies of the mica polymorphs. Mineralogical Magazine, 31, 209–235.

Steiner, A. (1968) Clay minerals in hydrothermally altered rocks at Wairakei, New Zealand. Clays and Clay Minerals, 16, 193–213.

Velde, B. (1965) Experimental determination of muscovite polymorph stabilities. American Mineralogist, 50, 436–449.

Wagner, C. (1961) Theorie der Alterung von Neiderschlägen durch Umlösen (Ostwald Reifung). Zeitschrift für Electrochemie, 65, 581–591.

Watanabe, T. (1981) Identification of illite/montmorillonite interstratifications by X-ray powder diffraction. Journal of the Mineralogical Society of Japan, Special Issue 15, 32–41 (in Japanese).

Weaver, C.E., and Beck, K.C. (1971) Clay water diagenesis during burial: How mud becomes gneiss. Geological Society of America Special Paper 134, 1–78.

Yoder, H.S., Jr., and Eugster, H.P. (1955) Synthetic and natural muscovites. Geochemica et Cosmochimica Acta, 8, 225–280.

Manuscript received February 29, 1988
Manuscript accepted July 1, 1988